PLOS ONE

RESEARCH ARTICLE

Anisotropic shortening in the wavelength of electrical waves promotes onset of electrical turbulence in cardiac tissue: An *in silico* study

Soling Zimik[1], **Rahul Pandit**[1], **Rupamanjari Majumder**[2]*

1 Centre for Condensed Matter Theory, Department of Physics, Indian Institute of Science, Bangalore, India, **2** Laboratory for Fluid Physics, Pattern Formation and Biocomplexity, Max Planck Institute for Dynamics and Self-Organization, Göttingen, Germany

* rupamanjari.majumder@ds.mpg.de

Citation: Zimik S, Pandit R, Majumder R (2020) Anisotropic shortening in the wavelength of electrical waves promotes onset of electrical turbulence in cardiac tissue: An *in silico* study. PLoS ONE 15(3): e0230214. https://doi.org/10.1371/journal.pone.0230214

Editor: Elena G. Tolkacheva, University of Minnesota, UNITED STATES

Received: October 22, 2019

Accepted: February 24, 2020

Published: March 13, 2020

Data Availability Statement: All relevant data are within the paper and its Supporting Information files.

Funding: This study was funded by Council of Scientific and Industrial Research (CSIR, India) and the Department of Science and Technology (DST, India).

Competing interests: The authors have declared that no competing interests exist.

Abstract

Several pathological conditions introduce spatial variations in the electrical properties of cardiac tissue. These variations occur as localized or distributed gradients in ion-channel functionality over extended tissue media. Electrical waves, propagating through such affected tissue, demonstrate distortions, depending on the nature of the ionic gradient in the diseased substrate. If the degree of distortion is large, reentrant activity may develop, in the form of rotating spiral (2d) and scroll (3d) waves of electrical activity. These reentrant waves are associated with the occurrence of lethal cardiac rhythm disorders, known as arrhythmias, such as ventricular tachycardia (VT) and ventricular fibrillation (VF), which are believed to be common precursors of sudden cardiac arrest. By using state-of-the-art mathematical models for generic, and ionically-realistic (human) cardiac tissue, we study the detrimental effects of these ionic gradients on electrical wave propagation. We propose a possible mechanism for the development of instabilities in reentrant wave patterns, in the presence of ionic gradients in cardiac tissue, which may explain how one type of arrhythmia (VT) can degenerate into another (VF). Our proposed mechanism entails anisotropic reduction in the wavelength of the excitation waves because of anisotropic variation in its electrical properties, in particular the action potential duration (*APD*). We find that the variation in the *APD*, which we induce by varying ion-channel conductances, imposes a spatial variation in the spiral- or scroll-wave frequency ω. Such gradients in ω induce anisotropic shortening of wavelength of the spiral or scroll arms and eventually leads to instabilitites.

Introduction

Nonlinear waves in the form of spirals occur in many excitable media, examples of which include Belousov-Zhabotinsky-type systems [1], calcium-ion waves in *Xenopus* oocytes [2], the aggregation of *Dictyostelium discoideum* by cyclic-AMP signaling [3], the oxidation of carbon monoxide on a platinum surface [4], and, most important of all, cardiac tissue [5]. Understanding the development of such spiral waves and their spatiotemporal evolution is an

important challenge in the study of extended dynamical systems, in general, and especially in cardiac tissue, where these waves are associated with abnormal rhythm disorders, which are also called arrhythmias. Cardiac tissue can support many patterns of nonlinear waves of electrical activation, like traveling waves, target waves, and spiral and scroll waves [6]. The occurrence of spiral- and scroll-wave turbulence of electrical activation in cardiac tissue has been implicated in the precipitation of life-threatening cardiac arrhythmias like ventricular tachycardia (VT) and ventricular fibrillation (VF), which destroy the regular rhythm of a mammalian heart and render it incapable of pumping blood. These arrhythmias are the leading cause of death in the industrialized world [7–11].

Biologically, VF can arise because of many complex mechanisms. Some of these are associated with the development of instability-induced spiral- or scroll-wave turbulence [12]. One such instability-inducing factor is ionic heterogeneity [13, 14], which arises from variations in the electrophysiological properties of cardiac cells (myocytes), like the morphology and duration of their action-potentials (*AP*s) [15–18]. Such variations may appear in cardiac tissue because of electrical remodeling [19–21], induced by alterations in ion-channel expression and activity, which arise, in turn, from diseases [22] like ischemia [23, 24], some forms of cardiomyopathy [25], and the long-QT syndrome [26]. To a certain extent, some heterogeneity is normal in healthy hearts; and it has an underlying physiological purpose [16, 27–31]; but, if the degree of heterogeneity is more than is physiologically normal, it can be arrhythmogenic [20, 24, 32]. It is important, therefore, to explore ionic-heterogeneity-induced spiral- or scroll-wave turbulence in mathematical models of cardiac tissue, which allow us to control this heterogeneity precisely, in order to be able to identify the nonlinear-wave instability that leads to such turbulence. We initiate such a study by examining the effects of this type of heterogeneity in three cardiac-tissue models, which are, in order of increasing complexity and biological realism, (a) the two-variable Aliev-Panfilov model [33], (b) the ionically realistic O'Hara-Rudy (ORd) model [34] in two dimensions (2D), and (c) the ORd model in an anatomically realistic simulation domain. In each one of these models, we control parameters (see below) in such a way that the ion-channel properties change anisotropically in our simulation domains, thereby inducing an anisotropic spatial variation in the local action potential duration *APD*. We show that this variation in the *APD* leads, in all these models, to an anisotropic reduction of the wavelength of the spiral or scroll waves; and this anisotropic reduction of the wavelength paves the way for an instability that precipitates turbulence, the mathematical analog of VF, in these models.

Materials and methods

The Aliev-Panfilov model provides a simplified description of an excitable cardiac cell [33]. It comprises a set of coupled ordinary differential equations (ODEs), for the normalized representations of the transmembrane potential V and the generalized conductance r of the slow, repolarizing current:

$$\frac{dV}{dt} = -kV(V-a)(V-1) - Vr; \tag{1}$$

$$\frac{dr}{dt} = [\epsilon + \frac{\mu_1 r}{\mu_2 + V}][-r - kV(V-b-1)]; \tag{2}$$

fast processes are governed by the first term in Eq (1), whereas, the slow, recovery phase of the *AP* is determined by the function $\epsilon + \frac{\mu_1 r}{\mu_2 + V}$ in Eq (2). The parameter a represents the threshold of activation and k controls the magnitude of the transmembrane current. We use the standard

values for all parameters [33], except for the parameter k. We write $k = g \times k_o$, where g is a multiplication factor and k_o is the control value of k. In 2D simulations we introduce a spatial gradient (a linear variation) in the value of k along the vertical direction of the domain. To mimic the electrophysiology of a human ventricular cell, we perform similar studies using a slightly modified version of the ionically-realistic O'Hara-Rudy model (ORd) [34, 35]. Here, the transmembrane potential V is governed by the ODE

$$\frac{dV}{dt} = -\frac{I_{\text{ion}}}{C_m}, \qquad I_{ion} = \Sigma_x I_x, \tag{3}$$

where I_x, the membrane ionic current, for a generic ion channel x, of a cardiac cell, is

$$I_x = G_x f_1(p_{act}) f_2(p_{inact})(V_m - E_x), \tag{4}$$

where $C_m = 1\ \mu$F is the membrane capacitance, $f_1(p_{act})$ and $f_2(p_{inact})$ are, respectively, functions of probabilities of activation (p_{act}) and inactivation (p_{inact}) of the ion channel x, and E_x is its Nernst potential. We give a list of all the ionic currents in the ORd model in Table 1. We write $G_i = g \times G_{io}$, where G_{io} is the original value of the maximal conductance of the ion channel x in the ORd model, and g is a multiplication factor. We model gradients in G_i as follows:

$$G_i(y) = [g_{min} + \frac{y(g_{max} - g_{min})}{L}]G_{io}, 0 \leq y \leq L; \tag{5}$$

here, L is the length of the side of the square simulation domain, and g_{max} and g_{min} are, respectively, the maximal and minimal values of g; we can impose gradients in k in the Aliev-Panfilov model in the same manner. For simplicity, we induce the gradient along one spatial direction only: the vertical axis in 2D; and the apico-basal (apex-to-base) direction in 3D. The spatiotemporal evolution of V in both models is governed by the following reaction-diffusion equation:

$$\frac{\partial V}{\partial t} + I = \nabla.(\mathcal{D}\nabla V), \tag{6}$$

where $\mathcal{D}$ is the diffusion tensor, and $I = \frac{I_{\text{ion}}}{C_m}$ and $kV(V-a)(V-1) + Vr$ for ORd and Aliev-Panfilov models, respectively. For the numerical implementation of the diffusion term in Eq (6), we follow Refs. [35, 36]. We construct our anatomically realistic simulation domain with

Table 1. The various ionic currents incorporated in the ORd model are tabulated above. The symbols used for the currents follow Ref. [34].

I_{Na}	fast inward Na^+ current
I_{to}	transient outward K^+ current
I_{CaL}	L-type Ca^{2+} current
I_{Kr}	rapid delayed rectifier K^+ current
I_{Ks}	slow delayed rectifier K^+ current
I_{K1}	inward rectifier K^+ current
I_{NaCa}	Na^+/Ca^{2+} exchange current
I_{NaK}	Na^+/K^+ ATPase current
I_{Nab}	Na^+ background current
I_{Cab}	Ca^{2+} background current
I_{pCa}	sarcolemmal Ca^{2+} pump current
I_{Kb}	K^+ background current
I_{CaNa}	Na^+ current through the L-type Ca^{2+} channel
I_{CaK}	K^+ current through the L-type Ca^{2+} channel

https://doi.org/10.1371/journal.pone.0230214.t001

processed human-ventricular data, obtained by using Diffusion Tensor Magnetic Resonance Imaging (DTMRI) [37]. For our 2D isotropic-domain with ORd model, we set $D = 0.0012 cm^2/ms$. The temporal and spatial resolutions are set to be $\delta x = 0.02$ cm and $\delta t = 0.02$ ms, respectively, and all the simulations are performed in a domain with 960 × 960 grid points. For the anatomically-realistic domain, we use a phase-field method for the boundary conditions [38]. The value of diffusion constant along the fiber ($D_{\parallel}$) is set equal to the value of D in the 2D isotropic case (i.e., 0.0012 cm^2/ms) and its value perpendicular ($D_{\perp}$) to the fiber is 1/4 times $D_{\parallel}$. The simulation is performed in a cubical domain with 512^3 grid points with the same spatial and temporal resolutions that we use in our 2D simulations. We do not incorporate the intrinsic ionic heterogeneities that are present in real mammalian hearts [16, 27–31]. In our single-cell simulations, the APD is calculated by measuring the duration over which the cell depolarizes and repolarizes to 90% (APD_{90}) of its peak transmembrane voltage in the action potential.

Results

Spiral-wave instability

In Fig 1(a) we show the variation, with the parameter g, of $\overline{APD} = APD/APD_o$, where APD_o is the control APD value for $g = 1$. We find that $\overline{APD}$ decreases with increasing g. Changes in the APD at the single-cell level influence electrical-wave dynamics at the tissue level. In particular, such changes affect the rotation frequency ω of reentrant activity (spiral waves). If θ and λ denote, respectively, the conduction velocity and wavelength of a plane electrical wave in tissue, then $\omega \simeq \frac{\theta}{\lambda}$, $\lambda \simeq \theta \times APD$. Therefore, if we neglect the effects of curvature [39] and

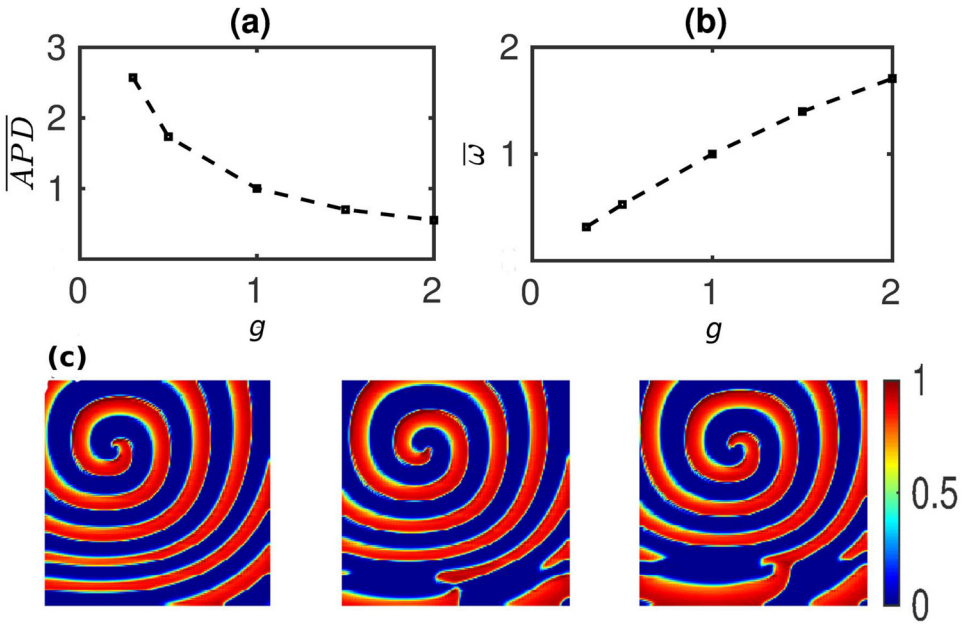

Fig 1. Occurrence of spiral-wave instability in a generic model of cardiac tissue with ionic heterogeneity. Variation of (a) $\overline{APD}$ and (b) $\overline{\omega}$ (see text) with k. $\overline{APD} = APD/APD_o$; here, APD_o is the control value of APD at $g = 1$ (so $\overline{APD} = 1$ at $g = 1$); we also use other combinations of ($\overline{APD}$, g) in our numerical simulations. We find that $\overline{APD}$ decreases with increasing k; however, $\overline{\omega}$ increases with increasing k. (c) Pseudocolor plots of V, at three representative times (time increases from left to right), illustrating the development of the spiral-wave instability in the Aliev-Panfilov model with a linear gradient in k; S1 Video in SI shows the complete spatiotemporal evolution of this instability.

https://doi.org/10.1371/journal.pone.0230214.g001

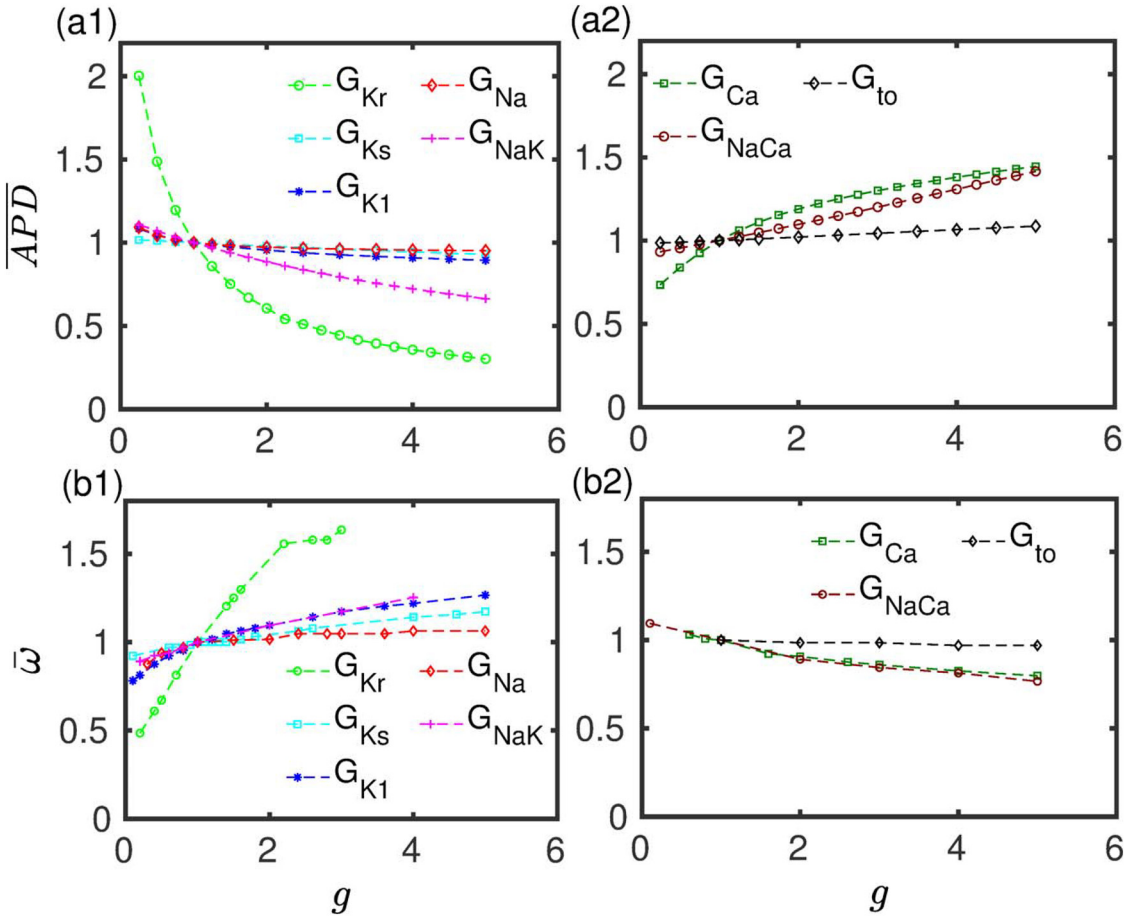

Fig 2. Variation of $\overline{APD}$ and $\overline{\omega}$ with various ionic cunductances. Plots of $\overline{APD}$ and $\overline{\omega}$ versus g; here, $\overline{APD} = APD/APD_o$ and $\overline{\omega} = \omega/\omega_0$, where APD_o = 250 ms, and ω_0 = 4.38 Hz are, respectively, the control values of APD and ω; (a1) and (a2) show, respectively, that $\overline{APD}$ decreases with the conductances G_i, for the currents I_{Kr}, I_{Ks}, I_{K1}, I_{Na} and I_{NaK}; however, it increases with increasing G_i, for the currents I_{CaL}, I_{NaCa} and I_{to}; (b1) and (b2) show that the variation of $\overline{\omega}$, with the various channel conductances, is consistent with Eq (2).

https://doi.org/10.1371/journal.pone.0230214.g002

excitable gap, the spiral-wave frequency

$$\omega \simeq \frac{1}{APD}. \tag{7}$$

We find, in agreement with this simple, analytical estimate, that ω decreases as the APD increases. We show this in Fig 1(b) by plotting $\overline{\omega} = \omega/\omega_0$ versus g; here, ω_0 is the frequency for g = 1. For the parameter a this simple relation between ω and APD is not observed, because change in a affects not only the APD but also other quantities like θ, which has effects on the value of ω. The spiral-wave frequency ω is obtained by simulating a spiral-wave in a homogeneous domain for every value of g.

Similarly, in the ionically realistic ORd model, changes in the ion-channel conductances G_i alter the APD of the cell and, therefore, the spiral-wave frequency ω. In Fig 2(a1) and 2(a2) we present a family of plots to illustrate the variation in $\overline{APD}$ with changes in G_i. We find that $\overline{APD}$ decreases with an increase in g for most currents (I_{Kr}, I_{Ks}, I_{K1}, I_{Na} and I_{NaK}); but it increases for some other currents (I_{Ca}, I_{NaCa} and I_{to}). The rate of change of $\overline{APD}$ is most significant when we change G_{Kr}; by contrast, it is most insensitive to changes in G_{Na} and G_{to}. In

Fig 2(b1) and 2(b2) we show the variation of $\overline{\omega}$ with g for different ion channels x. We find that changes in G_i, which increase *APD*, decrease ω and vice versa; this follows from Eq (2). The sensitivity of ω, with respect to changes in G_i, is most for $G_i = G_{Kr}$ and least for $G_i = G_{to}$: $\overline{\omega}$ *increases* by $\Delta\overline{\omega} \simeq 1.23$, as g goes from 0.2 to 5; for G_{to}, the same variation in g *decreases* the value of $\overline{\omega}$ by $\Delta\overline{\omega} \simeq 0.04$. We have done many simulations for each G_i with different values of $\Delta\overline{\omega}$ to check if a critical value $\Delta\overline{\omega}_c$ exists such that above (below) $\Delta\overline{\omega}_c$ we see wave breaks (no wave breaks) for all G_is. We find, however, that no such $\Delta\overline{\omega}_c$ exists, that is common for all G_is, which is because the stability of the spiral waves depends on the local values of the gradients in *APD*.

We now investigate the effects, on spiral-wave dynamics, of spatial gradients in k, in the 2D Aliev-Panfilov model, and in G_i, in the 2D ORd model. A linear gradient in k, in the Aliev-Panfilov model, induces a gradient in $\overline{\omega}$ (see Fig 1(b)); and such a spatial gradient in $\overline{\omega}$ induces a spiral-wave instability in the low-$\overline{\omega}$ region. In Fig 1(c) we demonstrate how a gradient in k ($g_{max} = 1.5$ and $g_{min} = 0.5$) leads to the precipitation of this instability (also see S1 Video).

Similarly, for each current listed in Table 1 for the ORd model, we find wave breaks in a medium with a gradient in G_i. We illustrate, in Fig 3, such wave breaks in our 2D simulation domain, with a gradient (∇G_i) in any G_i, for 3 representative currents; we select I_{Kr}, because it has the maximal impact on the single-cell *APD*, and also on ω in tissue simulations; and we choose I_{K1} and I_{NaCa}, because they have moderate and contrary effects on *APD* and ω (Fig 2). Our results indicate that gradient-induced wave breaks are generic, insofar as they occur in both the simple two-variable (Aliev-Panfilov) and the ionically realistic (ORd) models of cardiac tissue. In Fig 3(d)–(3f), we present power spectra of the time series of V, recorded from a representative point of the simulation domain; these spectra show broad-band backgrounds,

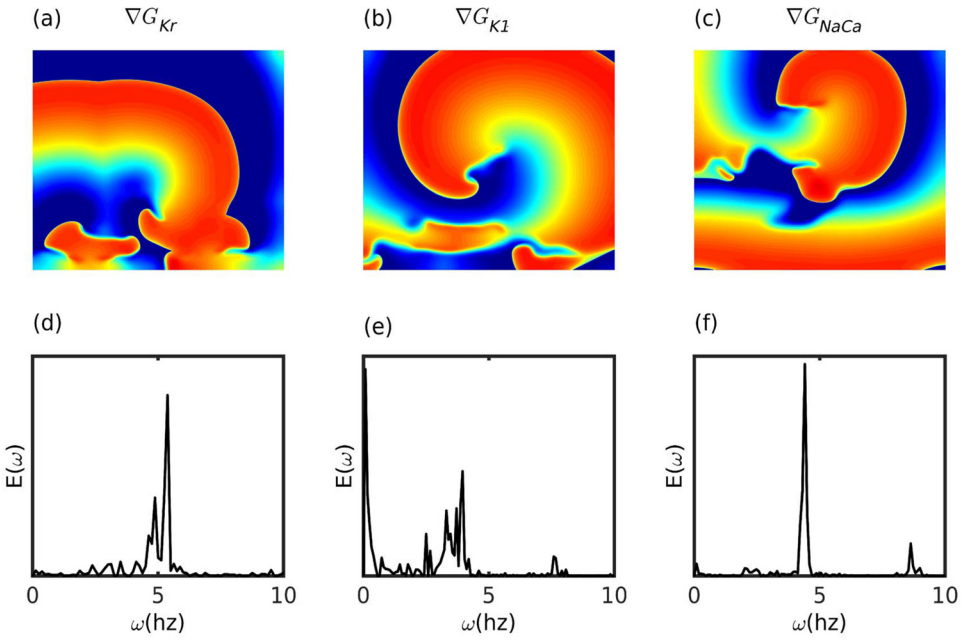

Fig 3. Spiral-wave instability. Pseudocolor plots of the transmembrane potential V_m illustrating spiral-wave instabilities from our numerical simulations of the 2D ORd model for human ventricular tissue, with spatial gradients in (a) G_{Kr}, (b) G_{K1}, and (c) G_{NaCa} (because G_{NaCa} decreases with g (Fig 2), the gradient in G_{NaCa} must be chosen to be the negative of that in Eq (5)); in (a)-(c) the local value of ω decreases from the top of the simulation domain to its bottom. Power spectra of the time series of V_m, from representative points in our simulation domain, are shown for gradients in (d) G_{Kr}, (e) G_{K1}, and (f) G_{NaCa}; the spectra in (d) and (e) are consistent with the onset of spiral-wave turbulence; the power spectrum in (f) shows the continuation of periodic electrical activity, in spite of wave breaks.

https://doi.org/10.1371/journal.pone.0230214.g003

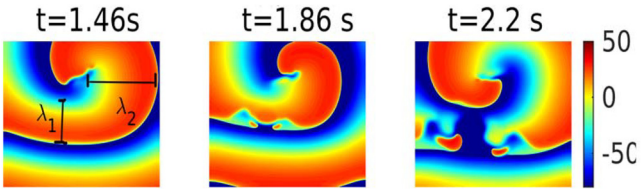

Fig 4. Mechanism of spiral-wave instability. Pseudocolor plots of V_m illustrating the development of a spiral-wave instability, with the passage of time t, in the 2D ORd model, with a spatial gradient in G_{NaCa}. The left frame shows the shortening of the spiral arm (λ varies along the spiral arm, and $\lambda_2 > \lambda_1$) indicated just before the spiral wave breaks (see the middle and the right frames).

https://doi.org/10.1371/journal.pone.0230214.g004

which are signatures of chaos, for the gradients ∇G_{Kr} and ∇G_{K1}; however, the gradient ∇G_{NaCa} induces wave breaks while preserving the periodicity of the resultant, reentrant electrical activity, at least at the points from which we have recorded V.

The instability in spiral waves occurs because spatial gradients in k (Aliev-Panfilov) or in G_i (ORd) induce spatial variations in both $\overline{APD}$ and $\overline{\omega}$: In our simulation domain, the local value of $\overline{\omega}$ ($\overline{APD}$) decreases (increases) from the top to the bottom. In the presence of a single spiral wave (left panel of Fig 4), the domain is paced, in effect, at the frequency ω of the spiral, i.e., with a fixed time period $T = 1/\omega = APD + DI$, where DI is the diastolic interval (the time between the repolarization of one AP and the initiation of the next AP). Thus, the bottom region, with a long APD, has a short DI and vice versa. The restitution of the conduction velocity θ implies that a small DI leads to a low value of θ and vice versa [40] (see Fig 5). To compensate for this reduction of θ, the spiral wave must reduce its wavelength λ, in the bottom, large-APD (small-DI) region, so that its rotation frequency $\omega \simeq \frac{\theta}{\lambda}$ remains unchanged, as shown in Fig 4 (also see S2 Video), where the shortening of the spiral arms is indicated by the variation

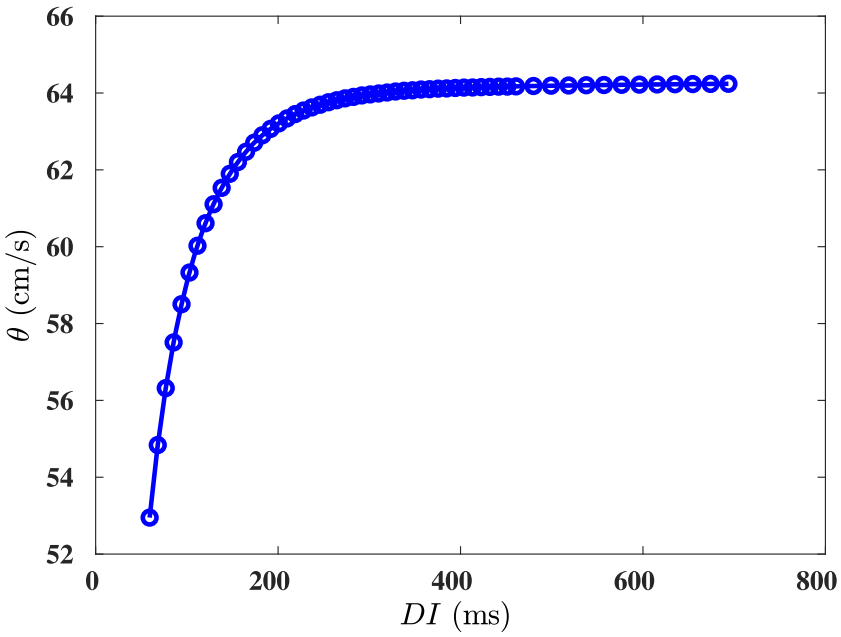

Fig 5. Cunduction-velocity (CV) restitution curve. Figure showing a CV restitution curve, generated by using the ORd model. The value of conduction velocity θ initially increases with the increase of diastolic interval DI and saturates at large values of DI.

https://doi.org/10.1371/journal.pone.0230214.g005

of λ along the spiral arm ($\lambda_2 > \lambda_1$, in the pseudocolor plot of V_m in the top-left panel $t = 1.46$ s). Clearly, this shortening is anisotropic, because of the uni-directional variation in k or G_i; this anisotropy creates functional heterogeneity in wave propagation, causing a local conduction block, which leads in turn to the spiral-wave instability we have discussed above (Fig 4). The phenomenon of conduction block in a medium with a gradient in ionic properties has been extensively investigated in an earlier study [41]; here, it is this local conduction block (caused by the anisotropy of the medium) that leads to the break-up of the spiral arms. It should be noted that the stability of the spiral wave depends on the APD difference between the region, where the spiral is initiated, and the top region, where the APD is maxmium; therefore, its stability depends on the location of the spiral-wave initiation along the vertical direction.

In the ORd model, we find that gradients in G_{Kr} easily induce instabilities of the spiral for small values of $\Delta g \equiv g_{max} - g_{min} \simeq 0.5$; by contrast, in a medium with gradients in G_{to}, the spiral remains stable for values of Δg as large as 4.8 (shown in Fig 6). This implies that the stability of the spiral depends on the magnitude of the gradient in ω that is induced in the medium.

Scroll-wave instability

In Fig 7 (also see S3 Video), we extend our study to illustrate the onset of scroll-wave instabilities in a 3D, anatomically realistic human-ventricular domain, in the presence of spatial gradients in G_{Kr}. In mammalian hearts, the *APD* is typically lower in the apical region as compared to that in the basal region [16]. Therefore, we use values of the *APD* that increase from the apex to the base (and, hence, ω decreases from the apex to base). With $g_{max}(G_{Kr}) = 6$ and $\Delta g = 4$, we observe breakup in a scroll wave that is otherwise stable in the absence of this spatial gradient. We note that the mechanism for the onset of such scroll-wave instabilities is the same as in 2D, and it relies on the gradient-induced anisotropic shortening of the scroll wavelength. For control, we also perform a simulation with small $\Delta g = 0.1$ that does not show scroll-wave instability (see S4 Video).

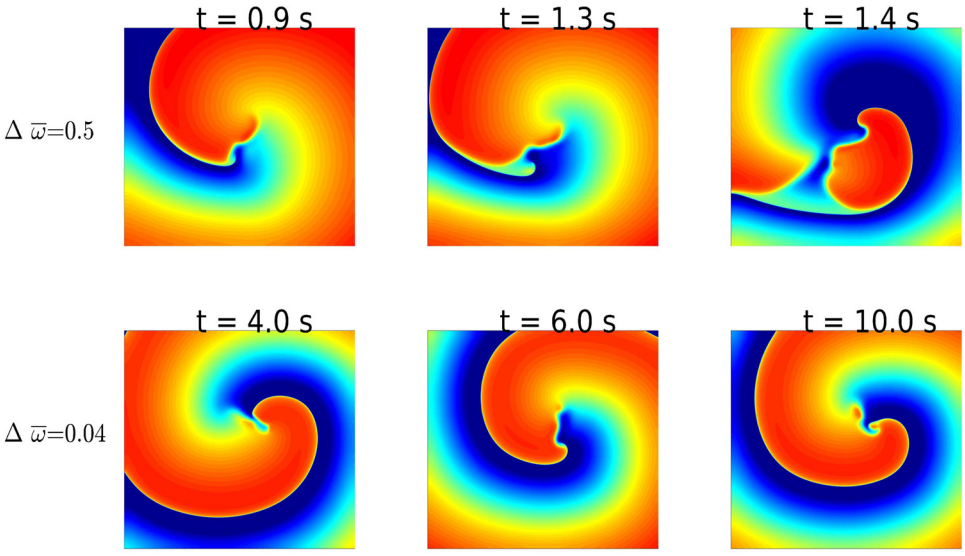

Fig 6. Dependence of spiral-wave stability on Δω. Pseudocolor plots of V_m illustrating the development of a spiral-wave instability for $\Delta\overline{\omega} = 0.5$ (top-row panels) and the sustenance of a stable spiral for $\Delta\overline{\omega} = 0.4$ (bottom-row panels). The parameter sets are as follows: top row, $\Delta g = 0.5$, $g_{min} = 0.5$ and $G_i = G_{Kr}$; bottom row, $\Delta g = 0.5$, $g_{min} = 0.2$ and $G_i = G_{to}$.

https://doi.org/10.1371/journal.pone.0230214.g006

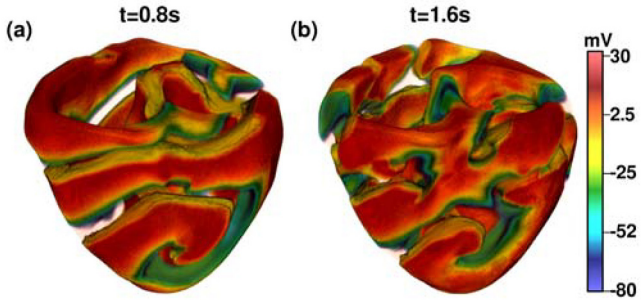

Fig 7. Scroll-wave instability. Pseudocolor plots of V_m illustrating the occurrence of scroll-wave instability in our anatomically realistic human-ventricular domain, in the presence of an apico-basal gradient in G_{Kr}.

https://doi.org/10.1371/journal.pone.0230214.g007

Discussion

We have shown that gradients in parameters that affect the *APD* of the constituent cells induce spatial gradients in the local value of ω. This gradient in the value of ω leads to an anisotropic reduction in the wavelength of the waves, because of the conduction-velocity restitution property of the tissue, and it paves the way for spiral- and scroll-wave instability in the domain. We would like to point out that this instability is not because of the condition of steep *APD* restitution curves as reported in ref. [12]. We find that the value of slopes of *APD* restitution curves for all values of g for all G_i in Fig 2 are less than one. Therefore, the instability of waves in our study is induced by the anisotropic variation of *APD* in the medium. This gradient-induced instability is a generic phenomenon because we obtain this instability in the simple Aliev-Panfilov and the detailed ORd model for cardiac tissue. Such an instability should be observable in any excitable medium that has the conduction-velocity-restitution property. We find that the spiral or scroll waves always break up in the low-ω region. This finding is in line with that of the experimental study by Campbell, *et al*., [15] on neonatal-rat-ventricular cell cultures and a computational study by Xie, *et al*., [42], who observe spiral-wave break-up in regions with a large *APD*. We find that the stability of the spiral is determined by the magnitude of the gradient in ω; the larger the magnitude of the gradient in the local value of ω, the more likely is the break up of the spiral or scroll wave. By using the ORd model, we find that ω varies most when we change G_{Kr} (as compared to other ion-channel conductances) and, therefore, spiral waves are most unstable in the presence of a gradient of G_{Kr}. By contrast, we find that ω varies most gradually with G_{to}, and hence the spiral wave is most stable in the presence of a gradient in G_{to} (as compared to gradients in other conductances).

Earlier studies have investigated the effects of ionic-heterogeneity on spiral-wave dynamics. The existence of regional ionic heterogeneities have been found to initiate spiral waves [43], attract spiral waves to the heterogeneity [44], and destabilize spiral waves [45]. The presence of *APD* gradients in cardiac tissue has been shown to drive spirals towards large-*APD* (low-ω) regions [46] or small- *APD* regions [47], called 'anomalous drift', by varying model parameters. We have also observed the drift of spiral waves towards the large-*APD* region (see Fig 8) in the initial time before the waves break up. A study by Zimik, *et al*., [35] finds that spatial gradients in ω, induced by gradients in the density of fibroblasts, can precipitate a spiral-wave instability. However, none of these studies provides a clear understanding of the mechanisms underlying the onset of spiral- and scroll-wave instabilities, from a fundamental standpoint. Moreover, none of these studies has carried out a detailed calculation of the pristine effects of each individual major ionic currents, present in a myocyte, on the spiral-wave frequency; nor have they investigated, in a controlled manner, how gradients in ion-channel conductances

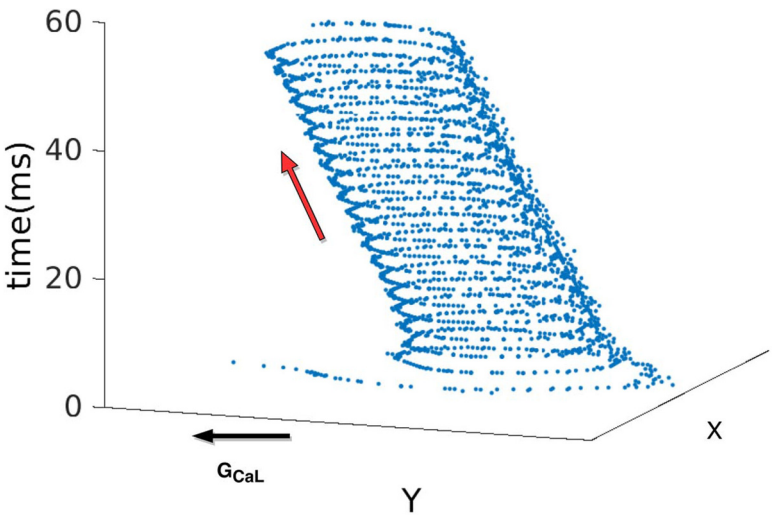

Fig 8. Spiral-wave drift towards low-ω region. Figure shows the loci of a spiral tip, which was tracked using the method in ref. [49]. Time is shown in the vertical axis and the X and Y axes are the spatial dimensions of our simulation domain. The gradient in ω is induced by applying a linear gradient in G_{CaL} along the Y axis (indicated by the black arrow), and the spiral drifts along the gradient as indicated by the red arrow. The g_{max} and g_{min} values are 3 and 1, respectively.

https://doi.org/10.1371/journal.pone.0230214.g008

lead to spiral- or scroll-wave instabilities. Our work makes up for these lacunae and leads to specific predictions that should be tested experimentally.

We end our paper by discussing certain limitations of our work. We have shown that large spatial gradients in *APD* can induce scroll-wave breaks in real hearts via a representative simulation on anatomically realistic heart domain with fiber orientation; however, we have not incorporated other important physiological details of real mammalian hearts, like the intrinsic heterogeneities that exists in them [16, 27–31], and the bidomain nature of the tissue [48]. Moreover, in our study we induce heterogeneity in the medium by applying a spatial gradient that extends throughout the domain, but, heterogeneities in real hearts tend to occur in localized regions. However, our results of spiral-wave break at large-*APD* region should still hold even if the heterogeneites are localized, as has been shown in [42].

Supporting information

S1 Video. Spiral-wave instability in the Aliev-Panfilov model. Video of pseudocolor plots of transmembrane potential V showing the formation of spiral-wave instability in a medium with gradient in k: $g_{min} = 0.5$ and $g_{max} = 1.5$. For the video, we use 10 frames per second with each frame separated from the succeeding frame by 20ms in real time.
(AVI)

S2 Video. Spiral-wave instability in the ORd model. Video pseudocolor plots of transmembrane potential V_m showing the formation of spiral-wave instability in a medium with a gradient in G_{Naca} ($g_{min} = 0.2$ and $g_{max} = 2$). For the video, we use 10 frames per second with each frame separated from the succeeding frame by 20ms in real time.
(AVI)

S3 Video. Scroll-wave instability. Video pseudocolor plots of transmembrane potential V_m showing the formation of scroll-wave instability in an anatomically realistic model for human ventricles. A linear gradient in G_{Kr} is applied along the apico-basal direction: $g_{min} = 2$ in the

apex and $g_{max} = 6$ in the base. For the video, we use 10 frames per second with each frame separated from the succeeding frame by 20ms in real time.
(AVI)

S4 Video. Stable scroll-wave. Video pseudocolor plots of transmembrane potential V_m showing a stable scroll-wave for small $\Delta g = 0.1$ in an anatomically realistic model for human ventricles. A linear gradient in G_{Kr} is applied along the apico-basal direction: $g_{min} = 2$ in the apex and $g_{max} = 2.1$ in the base. For the video, we use 10 frames per second with each frame separated from the succeeding frame by 20ms in real time.
(AVI)

Acknowledgments

We thank Mahesh Kumar Mulimani for important discussions that helped in improving the paper.

Author Contributions

Conceptualization: Soling Zimik, Rahul Pandit, Rupamanjari Majumder.

Data curation: Soling Zimik.

Formal analysis: Soling Zimik.

Investigation: Soling Zimik, Rupamanjari Majumder.

Methodology: Soling Zimik, Rupamanjari Majumder.

Project administration: Rahul Pandit, Rupamanjari Majumder.

Resources: Rahul Pandit.

Software: Rahul Pandit.

Supervision: Rahul Pandit, Rupamanjari Majumder.

Validation: Rupamanjari Majumder.

Visualization: Rupamanjari Majumder.

Writing – original draft: Soling Zimik, Rahul Pandit, Rupamanjari Majumder.

Writing – review & editing: Soling Zimik, Rahul Pandit, Rupamanjari Majumder.

References

1. Zaikin A, Zhabotinsky A. Concentration wave propagation in two-dimensional liquid-phase self-oscillating system. Nature. 1970; 225(5232):535. https://doi.org/10.1038/225535b0 PMID: 16056595
2. Clapham DE. Calcium signaling. Cell. 1995; 80(2):259–268. https://doi.org/10.1016/0092-8674(95)90408-5 PMID: 7834745
3. Tyson JJ, Murray J. Cyclic AMP waves during aggregation of Dictyostelium amoebae. Development. 1989; 106(3):421–426. PMID: 2557197
4. Imbihl R, Ertl G. Oscillatory kinetics in heterogeneous catalysis. Chemical Reviews. 1995; 95(3):697–733. https://doi.org/10.1021/cr00035a012
5. Davidenko JM, Pertsov AV, Salomonsz R, Baxter W, Jalife J. Stationary and drifting spiral waves of excitation in isolated cardiac muscle. Nature. 1992; 355(6358):349. https://doi.org/10.1038/355349a0 PMID: 1731248
6. Tyson JJ, Keener JP. Singular perturbation theory of traveling waves in excitable media (a review). Physica D: Nonlinear Phenomena. 1988; 32(3):327–361. https://doi.org/10.1016/0167-2789(88)90062-0

7. Bayly P, KenKnight B, Rogers J, Johnson E, Ideker R, Smith W. Spatial organization, predictability, and determinism in ventricular fibrillation. Chaos: An Interdisciplinary Journal of Nonlinear Science. 1998; 8(1):103–115. https://doi.org/10.1063/1.166291

8. Witkowski FX, Leon LJ, Penkoske PA, Giles WR, Spano ML, Ditto WL, et al. Spatiotemporal evolution of ventricular fibrillation. Nature. 1998; 392(6671):78–82. https://doi.org/10.1038/32170 PMID: 9510250

9. Walcott GP, Kay GN, Plumb VJ, Smith WM, Rogers JM, Epstein AE, et al. Endocardial wave front organization during ventricular fibrillation in humans. Journal of the American College of Cardiology. 2002; 39(1):109–115. https://doi.org/10.1016/s0735-1097(01)01696-5 PMID: 11755295

10. Efimov IR, Sidorov V, Cheng Y, Wollenzier B. Evidence of Three-Dimensional Scroll Waves with Ribbon-Shaped Filament as a Mechanism of Ventricular Tachycardia in the Isolated Rabbit Heart. Journal of cardiovascular electrophysiology. 1999; 10(11):1452–1462. https://doi.org/10.1111/j.1540-8167.1999.tb00204.x PMID: 10571365

11. De Bakker J, Van Capelle F, Janse M, Wilde A, Coronel R, Becker A, et al. Reentry as a cause of ventricular tachycardia in patients with chronic ischemic heart disease: electrophysiologic and anatomic correlation. Circulation. 1988; 77(3):589–606. https://doi.org/10.1161/01.cir.77.3.589 PMID: 3342490

12. Fenton FH, Cherry EM, Hastings HM, Evans SJ. Multiple mechanisms of spiral wave breakup in a model of cardiac electrical activity. Chaos: An Interdisciplinary Journal of Nonlinear Science. 2002; 12(3):852–892. https://doi.org/10.1063/1.1504242

13. Moe GK, Rheinboldt WC, Abildskov J. A computer model of atrial fibrillation. American heart journal. 1964; 67(2):200–220. https://doi.org/10.1016/0002-8703(64)90371-0 PMID: 14118488

14. Jalife J. Ventricular fibrillation: mechanisms of initiation and maintenance. Annual review of physiology. 2000; 62(1):25–50. https://doi.org/10.1146/annurev.physiol.62.1.25 PMID: 10845083

15. Campbell K, Calvo CJ, Mironov S, Herron T, Berenfeld O, Jalife J. Spatial gradients in action potential duration created by regional magnetofection of hERG are a substrate for wavebreak and turbulent propagation in cardiomyocyte monolayers. The Journal of physiology. 2012; 590(24):6363–6379. https://doi.org/10.1113/jphysiol.2012.238758 PMID: 23090949

16. Szentadrassy N, Banyasz T, Biro T, Szabo G, Toth BI, Magyar J, et al. Apico–basal inhomogeneity in distribution of ion channels in canine and human ventricular myocardium. Cardiovascular Research. 2005; 65(4):851–860. https://doi.org/10.1016/j.cardiores.2004.11.022 PMID: 15721865

17. Stoll M, Quentin M, Molojavyi A, Thämer V, Decking UK. Spatial heterogeneity of myocardial perfusion predicts local potassium channel expression and action potential duration. Cardiovascular research. 2007;. https://doi.org/10.1093/cvr/cvm060 PMID: 18006439

18. Liu DW, Antzelevitch C. Characteristics of the Delayed Rectifier Current (IKr and IKs) in Canine Ventricular Epicardial, Midmyocardial, and Endocardial Myocytes A Weaker IKs Contributes to the Longer Action Potential of the M Cell. Circulation research. 1995; 76(3):351–365. https://doi.org/10.1161/01.res.76.3.351 PMID: 7859382

19. Elshrif MM, Shi P, Cherry EM. Representing Variability and Transmural Differences in a Model of Human Heart Failure. IEEE journal of biomedical and health informatics. 2015; 19(4):1308–1320. https://doi.org/10.1109/JBHI.2015.2442833 PMID: 26068919

20. Nattel S, Maguy A, Le Bouter S, Yeh YH. Arrhythmogenic ion-channel remodeling in the heart: heart failure, myocardial infarction, and atrial fibrillation. Physiological reviews. 2007; 87(2):425–456. https://doi.org/10.1152/physrev.00014.2006 PMID: 17429037

21. Cutler MJ, Jeyaraj D, Rosenbaum DS. Cardiac electrical remodeling in health and disease. Trends in pharmacological sciences. 2011; 32(3):174–180. https://doi.org/10.1016/j.tips.2010.12.001 PMID: 21316769

22. Amin AS, Tan HL, Wilde AA. Cardiac ion channels in health and disease. Heart Rhythm. 2010; 7(1):117–126. https://doi.org/10.1016/j.hrthm.2009.08.005 PMID: 19875343

23. Harken AH, Barlow CH, Harden WR, Chance B. Two and three dimensional display of myocardial ischemic "border zone" in dogs. The American journal of cardiology. 1978; 42(6):954–959. https://doi.org/10.1016/0002-9149(78)90681-1 PMID: 215026

24. Jie X, Trayanova NA. Mechanisms for initiation of reentry in acute regional ischemia phase 1B. Heart Rhythm. 2010; 7(3):379–386. https://doi.org/10.1016/j.hrthm.2009.11.014 PMID: 20097623

25. Sivagangabalan G, Nazzari H, Bignolais O, Maguy A, Naud P, Farid T, et al. Regional Ion Channel Gene Expression Heterogeneity and Ventricular Fibrillation Dynamics in Human Hearts. PLoS ONE. 2014; 9(1):e82179. https://doi.org/10.1371/journal.pone.0082179 PMID: 24427266

26. Viswanathan PC, Rudy Y. Cellular arrhythmogenic effects of congenital and acquired long-QT syndrome in the heterogeneous myocardium. Circulation. 2000; 101(10):1192–1198. https://doi.org/10.1161/01.cir.101.10.1192 PMID: 10715268

27. Antzelevitch C, Sicouri S, Litovsky SH, Lukas A, Krishnan SC, Di Diego JM, et al. Heterogeneity within the ventricular wall. Circ Res. 1991; 69(6):1427–1449. https://doi.org/10.1161/01.res.69.6.1427 PMID: 1659499

28. Furukawa T, Myerburg RJ, Furukawa N, Bassett AL, Kimura S. Differences in transient outward currents of feline endocardial and epicardial myocytes. Circulation Research. 1990; 67(5):1287–1291. https://doi.org/10.1161/01.res.67.5.1287 PMID: 2225360

29. Fedida D, Giles W. Regional variations in action potentials and transient outward current in myocytes isolated from rabbit left ventricle. The Journal of Physiology. 1991; 442:191. https://doi.org/10.1113/jphysiol.1991.sp018789 PMID: 1665856

30. Zicha S, Xiao L, Stafford S, Cha TJ, Han W, Varro A, et al. Transmural expression of transient outward potassium current subunits in normal and failing canine and human hearts. The Journal of physiology. 2004; 561(3):735–748. https://doi.org/10.1113/jphysiol.2004.075861 PMID: 15498806

31. Samie FH, Berenfeld O, Anumonwo J, Mironov SF, Udassi S, Beaumont J, et al. Rectification of the background potassium current a determinant of rotor dynamics in ventricular fibrillation. Circulation research. 2001; 89(12):1216–1223. https://doi.org/10.1161/hh2401.100818 PMID: 11739288

32. Janse MJ. Electrophysiological changes in heart failure and their relationship to arrhythmogenesis. Cardiovascular research. 2004; 61(2):208–217. https://doi.org/10.1016/j.cardiores.2003.11.018 PMID: 14736537

33. Aliev RR, Panfilov AV. A simple two-variable model of cardiac excitation. Chaos, Solitons & Fractals. 1996; 7(3):293–301. https://doi.org/10.1016/0960-0779(95)00089-5

34. O'Hara T, Virág L, Varró A, Rudy Y. Simulation of the undiseased human cardiac ventricular action potential: model formulation and experimental validation. PLoS Comput Biol. 2011; 7(5):e1002061. https://doi.org/10.1371/journal.pcbi.1002061 PMID: 21637795

35. Zimik S, Pandit R. Instability of spiral and scroll waves in the presence of a gradient in thefibroblast density: the effects offibroblast–myocyte coupling. New J Phys. 2016; 18:123014. https://doi.org/10.1088/1367-2630/18/12/123014

36. Majumder R, Pandit R, Panfilov AV. Scroll-wave dynamics in the presence of ionic and conduction inhomogeneities in an anatomically realistic mathematical model for the pig heart. JETP letters. 2016; 104(11):796–799. https://doi.org/10.1134/S0021364016230041

37. DTMRI Data From Ex-Vivo Canine and Human Hearts, The CardioVascular Research Grid (http://cvrgrid.org/data/ex-vivo).;.

38. Fenton FH, Cherry EM, Karma A, Rappel WJ. Modeling wave propagation in realistic heart geometries using the phase-field method. Chaos: An Interdisciplinary Journal of Nonlinear Science. 2005; 15(1):013502. https://doi.org/10.1063/1.1840311

39. Qu Z, Xie F, Garfinkel A, Weiss JN. Origins of spiral wave meander and breakup in a two-dimensional cardiac tissue model. Annals of biomedical engineering. 2000; 28(7):755–771. https://doi.org/10.1114/1.1289474 PMID: 11016413

40. Cherry EM, Fenton FH. Suppression of alternans and conduction blocks despite steep APD restitution: electrotonic, memory, and conduction velocity restitution effects. American Journal of Physiology-Heart and Circulatory Physiology. 2004; 286(6):H2332–H2341. https://doi.org/10.1152/ajpheart.00747.2003 PMID: 14751863

41. Qu Z, Garfinkel A, Weiss JN. Vulnerable window for conduction block in a one-dimensional cable of cardiac cells, 1: single extrasystoles. Biophysical journal. 2006; 91(3):793–804. https://doi.org/10.1529/biophysj.106.080945 PMID: 16679367

42. Xie F, Qu Z, Garfinkel A, Weiss JN. Electrophysiological heterogeneity and stability of reentry in simulated cardiac tissue. American Journal of Physiology-Heart and Circulatory Physiology. 2001; 280(2):H535–H545. https://doi.org/10.1152/ajpheart.2001.280.2.H535 PMID: 11158949

43. Defauw A, Dawyndt P, Panfilov AV. Initiation and dynamics of a spiral wave around an ionic heterogeneity in a model for human cardiac tissue. Physical Review E. 2013; 88(6):062703. https://doi.org/10.1103/PhysRevE.88.062703

44. Defauw A, Vandersickel N, Dawyndt P, Panfilov AV. Small size ionic heterogeneities in the human heart can attract rotors. American Journal of Physiology-Heart and Circulatory Physiology. 2014; 307(10):H1456–H1468. https://doi.org/10.1152/ajpheart.00410.2014 PMID: 25217650

45. Xu A, Guevara MR. Two forms of spiral-wave reentry in an ionic model of ischemic ventricular myocardium. Chaos: An Interdisciplinary Journal of Nonlinear Science. 1998; 8(1):157–174. https://doi.org/10.1063/1.166286

46. Ten Tusscher K, Panfilov AV. Reentry in heterogeneous cardiac tissue described by the Luo-Rudy ventricular action potential model. American Journal of Physiology-Heart and Circulatory Physiology. 2003; 284(2):H542–H548. https://doi.org/10.1152/ajpheart.00608.2002 PMID: 12388228

47. Sridhar S, Sinha S, Panfilov AV. Anomalous drift of spiral waves in heterogeneous excitable media. Physical Review E. 2010; 82(5):051908. https://doi.org/10.1103/PhysRevE.82.051908

48. Henriquez CS. Simulating the electrical behavior of cardiac tissue using the bidomain model. Critical reviews in biomedical engineering. 1992; 21(1):1–77.

49. Qu Z, Weiss JN, Garfinkel A. Cardiac electrical restitution properties and stability of reentrant spiral waves: a simulation study. American Journal of Physiology-Heart and Circulatory Physiology. 1999; 276(1):H269–H283. https://doi.org/10.1152/ajpheart.1999.276.1.H269